

Vanadium-doped HfO₂, multiferroic uncompromised

Vincenzo Fiorentini,^{1,2} Paola Alippi,³ and Gianarelio Cuniberti²

¹*Department of Physics, University of Cagliari, Cittadella Universitaria, I-09042 Monserrato (CA), Italy*

²*Institute for Materials Science and Max Bergmann Center for Biomaterials, TU Dresden, D-01062 Dresden, Germany*

³*CNR-ISM, Istituto di Struttura della Materia, Area della ricerca Montelibretti, 00001 Monterotondo (RM), Italy*

(Dated: July 8, 2025)

Ab initio density-functional calculations show that orthorhombic $Pca2_1$ hafnia HfO₂ mixed with vanadium at low concentration is a ferroelectric and ferromagnetic insulator. The multiorbital degeneracy of singly-occupied V states in the nominally 4+ ionic state is broken by magnetism, reduced symmetry, and local distortion, causing a single one-electron majority state per V atom to be occupied. A gap of order 1 eV thus survives at all V concentrations, and intrinsic polarization is preserved, at the level of 60-70% of the hafnia value. Ferromagnetic magnetization is found to increase linearly with V content, with values of 30-40 emu/cm³ at concentrations near the end of the stability range ($\sim 16\%$ V).

I. INTRODUCTION

Multiferroics –materials in which multiple states of order coexist, such as ferroelectricity and some sort of magnetic order– are rare. Ferroelectrics that possess ferromagnetic order are even more rare, and usually only weakly ferromagnetic due to e.g. Dzyaloshinskii-Moriya-type interactions. In search for a more robust sort of multiferroicity, here we explore the doping of ferroelectric hafnia with a transition metal, signally V. As the stoichiometry is fixed by construction, one may also view this as the mixing of two materials each endowed with one of the requisite orders: the ferromagnet is VO₂ in its $C2/m$ monoclinic structure [1, 2] (more about this in Sec.II A); the ferroelectric is HfO₂ in the metastable (but amenable to stabilization) orthorhombic $Pca2_1$ structure [3]. The two are mixed into Hf_{1-x}V_xO₂ (or (Hf,V)O₂ for short) with x up to around 0.37. For this proof of concept, we assume the starting structure of hafnia, and analyze the energetics and a few relevant physical quantities (signally, magnetization and polarization), using a simple model to discuss stability against separation in bulk components. For the time being, we do not address the other end of the x range, where a non-polar or, potentially, metallic VO₂ state would probably dictate the structure.

The results, in a nutshell, are that polarization is conserved (though reduced) and magnetization increases linearly over the whole range considered; according to a model mixing free energy, the solid solution should be stable up to about $x=0.15$ at growth or annealing temperature 1000 K. The electronic structure evolves from the large gap of hafnia towards that of VO₂, with the appearance and progressive increase in weight of a V-related occupied density-of-states feature above the upper edge of the valence band. The geometry of V configurations seems to indicate a tendency to first form rows, then combinations of rows producing incomplete planes, then planes decorated by excess V, then V-rich regions separated by Hf-rich regions, causing the mixture to resemble a rough superlattice of hafnia and vanadia (typically

stacked along the crystal directions \mathbf{b} and, to a lesser extent, \mathbf{a}). Our findings seem to compare well with a very recent set of experiments on a device stack involving the solid solution [4].

II. METHODS

We calculate observables from first principles within density functional theory at multiple concentrations and for multiple configurations of V substituting for Hf in ferroelectric HfO₂. We use the VASP code (v.6.5) [5] and the PAW formalism [6] with the datasets V, Hf and O_s, at a cutoff of 350 eV (1.3 times the maximum recommended cutoff). The polarization is obtained by the Berry-phase method [7].

The density-functional calculations use spin-polarized GGA+U, i.e. the generalized gradient approximation (with the PBE [8] functional) with U corrections in the Dudarev version [9]. We set $U-J=3$ eV on V d states only, and no correction on all other channels. This choice is based on preliminary comparisons with hybrid functional calculations [10] for a few selected configurations at low V concentration, and is confirmed by previous reports [11]. This setting limits computational costs and makes it possible to study a large number of configurations. Several counterchecks with hybrid functionals confirm the findings of GGA+U. The main difference is the HfO₂ gap, smaller (4.9 eV in GGA+U and 5.9 in HSE, close to experiment) but still quite sufficient to capture the evolution of the electronic structure as function of V concentration.

The calculations are done in a supercell containing 32 cations and 64 anions (a $2\times 2\times 2$ replica of the $Pca2_1$ unit cell). In each configuration, V atoms substitute a random sample of n unique Hf atoms in the cell; n is between 1 and 12, corresponding to concentrations x between 0.031 and 0.375 in steps of 0.031. A total of 1481 configurations involving 9500 vanadium atoms are considered in the averages; the pairs ($n : N_{\text{conf}}$) are (2:130, 3:153, 4:165, 5:153, 6:131, 7:149, 8:145, 9:166, 10:75, 11:80, 12:80).

For $n=1$, we use 7 configurations, finding them identical to numerical accuracy as expected since all sites are equivalent.

The volume and internal geometry are optimized for each configuration using a $2 \times 2 \times 2$ k-space grid. Observables (energy, polarization, magnetization, dielectric function, Born charges) and density of states are then computed on a $4 \times 4 \times 4$ grid. (Finer grids are impractical given the relatively large cell and number of configurations). A Gaussian smearing of 0.02 eV is used. The various quantities presented below are obtained as configurational averages with the Boltzmann weights $\exp(E_i/k_B T_g)$ of the computed energies E_i and the assumed growth temperature $T_g=1000$ K (well within the range generally used for hafnia [12]; see also Sec.III E). The error bars in the Figures are obtained from the square root of the covariance matrix of the weighted quantities.

A. Magnetic insulator, general considerations

For polarization to be directly computable via the standard Berry-phase approach the system must remain insulating. If the local geometry were strictly octahedral, the excess valence electron of V would occupy a 6-fold degenerate t_{2g} state. A combination of "crystal-field" and magnetic level splitting is required to remove all degeneracies and open a gap in the spectrum. For example, in monoclinic $C2/m$ VO_2 the t_{2g} majority triplet splits [13] into an e_g^π doubly-degenerate state and an a_{1g} singly-degenerate state, which dominates the top valence bands. In $Pca2_1$ HfO_2 , whose point symmetry is $mm2$, the (majority) t_{2g} states are expected to split in three non-degenerate states a_1 , b_1 , and b_2 , and the e_g into a_1 and b_1 . Disorder by random V substitutions, and the attendant local distortions, about which more below, indeed formally remove all symmetries. As in VO_2 , the a_1 even state is expected to be lowest. Of course degeneracy removal requires a concurrent magnetic exchange splitting between the minority and majority channels, which is found to be approximately 2 to 4 eV in the present case. The end result is thus that a majority-channel gap (of order 1 eV) appears in the whole concentration range considered, separating occupied and empty V-derived states in the HfO_2 gap.

A small percentage of the configurations are found to be ferrimagnetic, with part of the V states involved being coupled antiferromagnetically. This results in a slight reduction of the average magnetization M from the ideally expected $1 \mu_B$ per V. For example, the most affected case is $n=4$ where 15 % of the configurations have $M=2 \mu_B$ instead of the $4 \mu_B$ expected for a full ferromagnet, and less than 1% have $M=0$. (M decreases by $2 \mu_B$ for each minority state going under the Fermi level.) The average magnetization per V is still a large $0.91 \mu_B$. The effect is less frequent at other concentrations, especially at the higher end. Indeed, the magnetization averaged over all

configurations is $0.957 \mu_B/V$, close to the maximum expected value of $1 \mu_B$.

Among our nearly 1500 configurations, we found 4 to be metallic. Such rare cases occur at low concentration, perhaps due to V impurities being accidentally related by some approximate symmetry, and we expect them to be irrelevant in the real material.

III. RESULTS

A. Bulk materials, formation energy and volume

The bulk materials are ferromagnetic VO_2 in the monoclinic $C2/m$ structure and ferroelectric HfO_2 in the (metastable) orthorhombic $Pca2_1$ structure. The former was shown to be treatable by density functional methods by Eyert [2]. The latter has been studied in many recent papers aiming at clarifying the nature of ferroelectricity [3] (about which we will have nothing to say, except that our setting does reproduce it). We start from configurations found in the Materials Project [14] (mp-685097 for HfO_2 and mp-541404 for VO_2) confirming them in our setting to within the usual accuracy of 1% or less in the lattice constants. The polarization in hafnia points along the \mathbf{b} crystal axis; the computed value for the $Pca2_1$ structure supercell (referred to its $P4_2nm$ symmetry parent) is smaller than obtained elsewhere [15], possibly due to a different reference or a relatively sparse k-sampling. This does not affect the general picture.

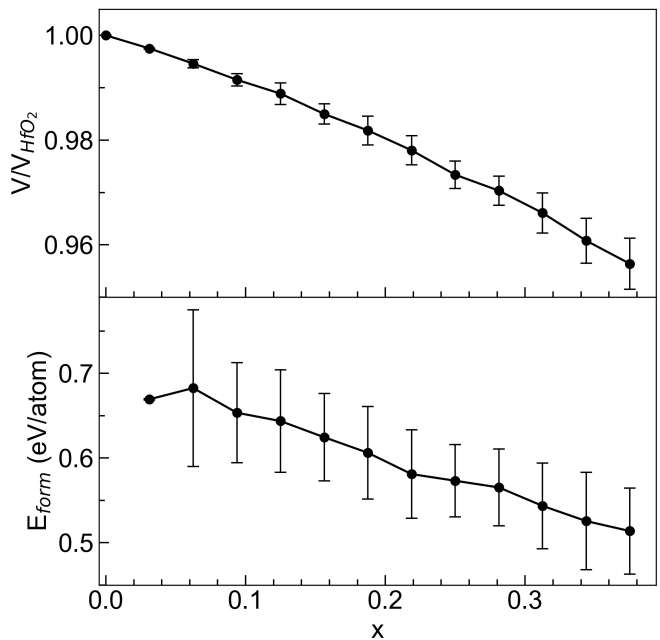


FIG. 1. Volume (top) and formation energy per V atom (bottom) of $(Hf,V)O_2$ vs concentration.

We elect to study a free-standing version of this system. Epitaxial constraints, sometimes used to stabilize

the ferroelectric phase, may be studied in forthcoming work. Figure 1, top panel, reports the volume of the simulation cell (top) vs concentration x . The volume reduction vs x is expected given the smaller volume per formula unit in VO_2 compared to HfO_2 in the same structure, although VO_2 in the $C2/m$ structure has a slightly (5%) larger specific volume. The relative variation of the three lattice constants is identical on average, i.e. the contraction is isotropic.

The bottom panel of Figure 1 reports the formation energy per atom of V in HfO_2 , obtained from the standard formula

$$E_f = [E_{(\text{Hf,V})\text{O}_2}(n) + n\mu_{\text{HfO}_2}] - [E_{\text{HfO}_2} + n\mu_{\text{VO}_2}] \quad (1)$$

with n the number of V atoms, μ_{HfO_2} and μ_{VO_2} the energy per formula unit of bulk HfO_2 and VO_2 , and $E_{(\text{Hf,V})\text{O}_2}$, and respectively E_{HfO_2} , the energy of the defected and undefected supercells. This yields a V concentration in HfO_2 in the mid 10^{19} cm^{-3} at 1000 K.

B. Mixing free energy and stability

To determine the stability of the solid solution we calculate its mixing free energy

$$\begin{aligned} F_{\text{mix}} &= F(x) - (1-x)F_{\text{HfO}_2} - xF_{\text{VO}_2} \quad (2) \\ &= E(x) - k_B T [S_m(x) + S_v(x)] \\ &\quad - (1-x)[E(0) - k_B T (S_m(0) + S_v(0))] \\ &\quad - x[\mu_{\text{VO}_2} - k_B T (S_m(1) + S_v(1))] \end{aligned}$$

where $x=n/N_{\text{Hf}}$ is the fractional occupation by V on the Hf lattice, with $N_{\text{Hf}}=32$ in our 96-atom simulation cell, $E(x)$ is the same as $E_{(\text{Hf,V})\text{O}_2}$ in Eq.1, and μ_{VO_2} is the bulk energy of $C2/m$ VO_2 as in Eq.1. For the entropy we adopt a standard approach [16] employed previously [17], whereby the mixing entropy is simply

$$S_m(x) = -x \log x - (1-x) \log(1-x)$$

and, since the Debye temperatures $\Theta_{\text{VO}_2}=750$ K and $\Theta_{\text{HfO}_2}=480$ K are both well below typical growth temperatures, the vibrational entropy is expressed in a single-oscillator approximation as

$$S_v(x) = 3[(1+n_B) \log(1+n_B) - n_B \log n_B]$$

where $n_B=1/(\exp[\Theta_x/T]-1)$ is the Bose distribution and $\Theta_x = (1-x)\Theta_{\text{HfO}_2} + x\Theta_{\text{VO}_2}$. The vibrational entropy, which is not symmetric in x and $(1-x)$, disfavors mixing at low x because the compound being admixed, VO_2 , is stiffer and has larger Debye energy (unlike in the $(\text{In,Ga})_2\text{O}_3$ case [17]).

The mixing free energy is shown in Figure 2, bottom panel (for the top panel see just below). The error bars, not shown to avoid clutter, are about $\pm 10\%$ of the plotted values. In order for the solid solution to be stable at a given x against phase separation in the constituent

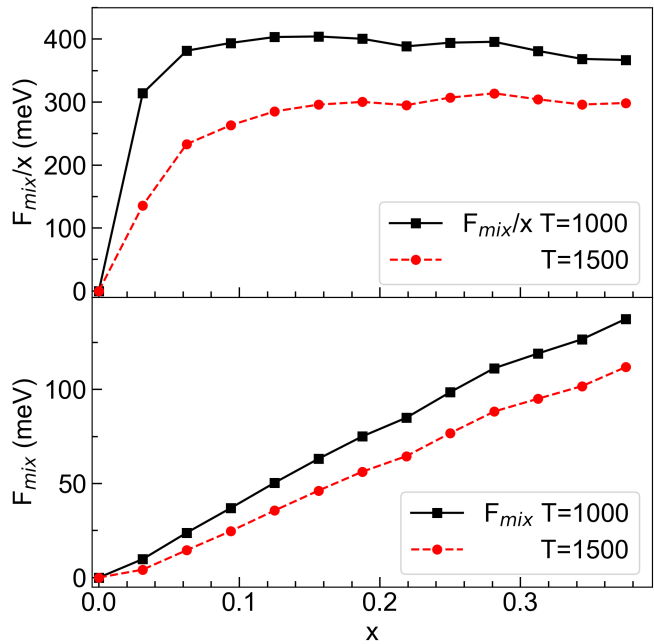


FIG. 2. F_{mix} (bottom) and F_{mix}/x (top) vs concentration at two temperatures. Error bars, not shown for clarity, are of order 10%.

bulks, the mixing free energy should have positive local curvature [16]. From the Figure this is difficult to judge, and taking derivatives is numerically inaccurate, so we try a visual heuristic. Consider $G(x)=F_{\text{mix}}(x)/x$, shown in Figure 2, top panel. If we assume $F \sim x^{\beta(x)}$ locally in x , the mixture is stable in x if $G \sim x^{\beta(x)-1}$ is upward convex and monotonically increasing. If so [18], $1 < \beta(x) < 2$ (e.g. the case of $G \sim \sqrt{x}$, i.e. $\beta(x)=3/2$), so that the local curvature $F_{xx} \sim \beta(x)(\beta(x)-1)x^{\beta(x)-2}$ is positive.

By this criterion, the stability range ends at $x \sim 0.16$ at 1000 K, and at $x \sim 0.19$ at 1500 K. After that, G becomes downward convex and/or decreasing, which means $\beta(x) < 1$ and hence negative curvature and instability.

C. Polarization and magnetization

Figure 3 reports the modulus $P=|\mathbf{P}|$ of the spontaneous polarization (top panel) and the magnetization M (bottom panel). The magnetization is close to its ideal value of $1 \mu_B$ per V, with downward fluctuations at low x as mentioned earlier, and leveling out asymptotically to the ideal value at large x ; the magnetization is treated as collinear, so there is no information about its direction (future work on non-collinearity and magnetoelectricity is planned).

P vs. x appears to saturate to about 70% of the HfO_2 value. There seems to be no systematic V-related mechanism of local dipole reduction. If V contributed less than Hf to P or subtracted from it (by e.g. a smaller Born charge or a displacement counter that of Hf in

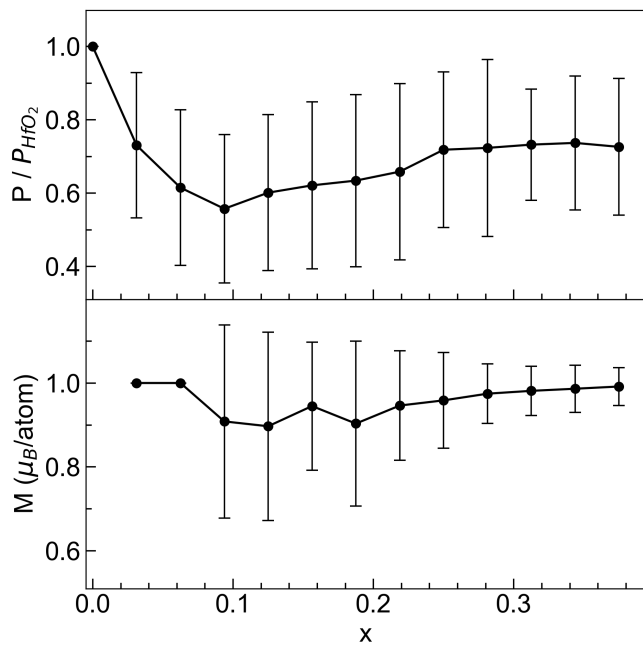


FIG. 3. Modulus of polarization (top) and magnetization (bottom) vs concentration.

the ferroelectric pattern), P should decrease with x . If only mostly-HfO₂ regions contributed to P and mostly-VO₂ regions did not (e.g. in the geometry of $n=12$ in Sec.III F), P should still decrease with x , being an extensive quantity.

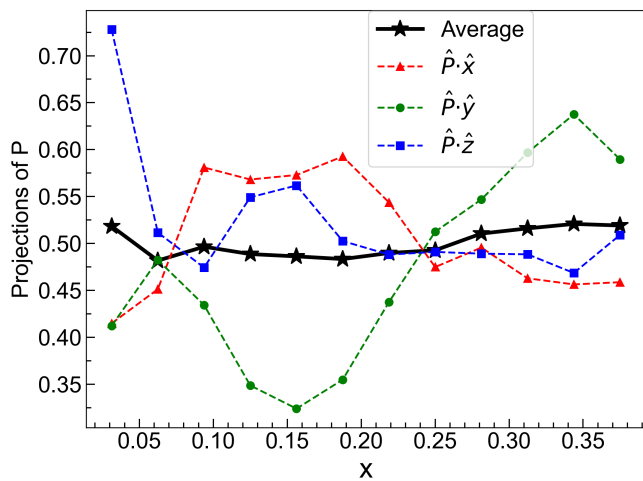


FIG. 4. Projection of the polarization vector on the Cartesian axes. The average projection corresponds roughly to a [111] direction.

Before attempting an interpretation, we provide info on the direction of \mathbf{P} . Figure 4 shows the configuration-averaged projections of the polarization vector $\hat{\mathbf{P}} = \mathbf{P}/P$ on the Cartesian vectors. For this orthorhombic system, this is equivalent to projecting on the crystal axes, nu-

merical factors aside. $\hat{\mathbf{P}}$ is parallel to $\hat{\mathbf{y}}$ at $x=0$, but of course it fluctuates considerably in the random configurations. Yet, an inspection of the configurations shows that *all* calculated \mathbf{P} vectors have positive Cartesian components, i.e. lie inside the first Cartesian octant, suggesting a systematic effect related to the underlying structure. Taking a further average of the averaged projections (solid line-and-stars in the Figure), one concludes that $\hat{\mathbf{P}}$ is, on average, very roughly parallel to the (111) crystal direction.

We suggest that the deviation of $\hat{\mathbf{P}}$ from $\hat{\mathbf{y}}$ in HfO₂ is explained by the underlying structure and local environment around Hf as modified by the substituting V. Hf has seven O neighbors, and V effectively loses one of them (the distance increases from ~ 2.2 Å to ~ 2.7 Å) forming a distorted octahedron with the remaining six. Two V-O bonds dimerize (relative difference $\sim 15\%$) along one of the octahedron's axes (which point roughly in the direction of the cell diagonals).

Now, in a naïve point-charge local-dipoles picture, a longer (oriented) O-to-V bond is a larger dipole than a shorter (oriented) O-to-V bond is, so the dimerization produces a net dipole pointing along the (oriented) V-to-O short bond. Examining our 9500 V substitutions, we find that all V octahedra are dimerized, and the configuration-averaged dipole direction points into the first Cartesian octant for all x . (Of course, this is not true of all configurations individually, although only about 1/4 of the bond vector components are negative.) Thus the dimerization distortion of the V octahedron contributes a dipole displacing \mathbf{P} off the y axis and into the first Cartesian octant.

Obviously the full polarization change will depend on the rearrangements of all atoms and on the changes in dynamical electronic response measured by the Born effective charges [7]. We calculate the Born tensors for $n=2, 5, 12$ (lowest energy configurations) to look for trends. Using as proxy the spherical component of the atom-averaged charge tensor (i.e. one third of its trace), we find an increase of the anomaly of the individual charges vs x : $Z_{\text{Hf}}=5.29, 5.37, 5.61$; $Z_{\text{O}}=-2.62, -2.62, -2.69$; and $Z_{\text{V}}=4.51, 4.56, 4.98$, for $x=0.03, 0.15, 0.36$ respectively. Finally, to measure the response at different x , we use the weighted cation charge $Z_c(x)=(1-x)Z_{\text{Hf}}+xZ_{\text{V}}(x)$ (the anion charge follows closely the acoustic sum rule $Z_c+2Z_a=0$). This is also found to increase with x , namely 5.238, 5.241, 5.377 for $x=0.03, 0.15, 0.36$. It thus appears that as x increases the Born charges of V and Hf remain sufficiently anomalous (in fact increasingly so) to produce an *increasing* effective charge anomaly.

To summarize our discussion, sustained dynamical charge anomalies and dipolar displacement patterns associated with V make it quite plausible that polarization be conserved in (Hf,V)O₂. (This is in line with [19] the *increased* polarization upon V doping of PbTiO₃ and the charge anomalies in V₂O₅ [20].)

D. Density of states and basic optical response

As mentioned in Sec.IIA, the origin of the insulating character of the solid solution is a combination of magnetic splitting and symmetry-lowering "crystal field" splitting (see also Sec.IIA). We now attempt a summary of some electronic structure features. For n ferromagnetic substituting V, we observe $10 \times n$ V d single-electron states in the HfO_2 gap, $5 \times n$ of which in the majority channel and as many in the minority. Exactly n non-degenerate majority states of V d character accommodate the n V electrons in a window about 0.5 to 1 eV wide just above the O-derived valence top of HfO_2 . The $4 \times n$ empty majority states are separated by a gap of over 1 eV, decreasing slowly at larger concentrations. In the minority channel, $5 \times n$ empty states appear at 2.5-3.5 eV from the occupied states. All of these features are indeed shared by the same energy region in ferromagnetic VO_2 .

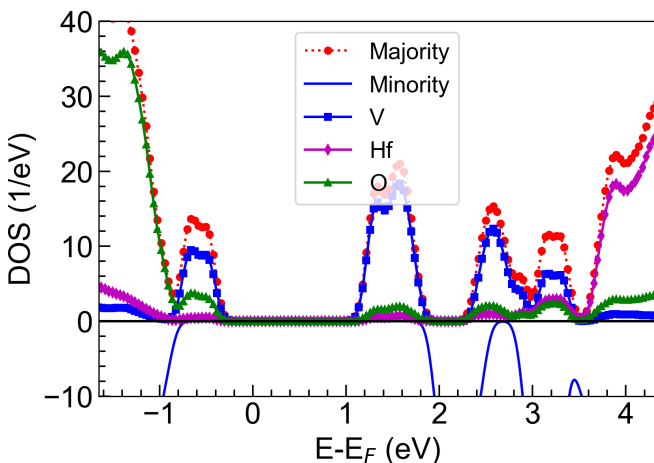


FIG. 5. Total and atom-projected DOS, $n=5$.

The magnetic separation, too small in GGA, is increased by GGA+U, which mimicks the selfinteraction cancellation of hybrid functionals [10] and selfinteraction-correction [21]. In fact, even GGA generally finds degeneracy removal and insulating character (with tiny gaps).

Inspecting various densities of states (DOS), we consistently find a gap of roughly 1 to 2 eV (larger at the lowest concentrations and configuration-dependent). The magnetic splitting is typically over 1 eV larger. Also, note the two lumps of empty V d states separated by about 1.5 eV, possibly a remnant $t_{2g}-e_g$ gap.

For definiteness, we visualize the DOS for the $x \approx 0.15$ lowest-energy configuration (in these Figures the Gaussian smearing is 0.1 eV). Figure 5 shows the near-gap region. The gap states are of almost pure V and O character, in a roughly 2:1 ratio for the occupied states, larger for the empty ones.

Figure 6 shows the DOS of the highest occupied states in the majority channel projected on the V atoms (again for $n=5$, $x \approx 15\%$) summed over the s , p , and d channels. The contributions of the five V atoms can be easily made

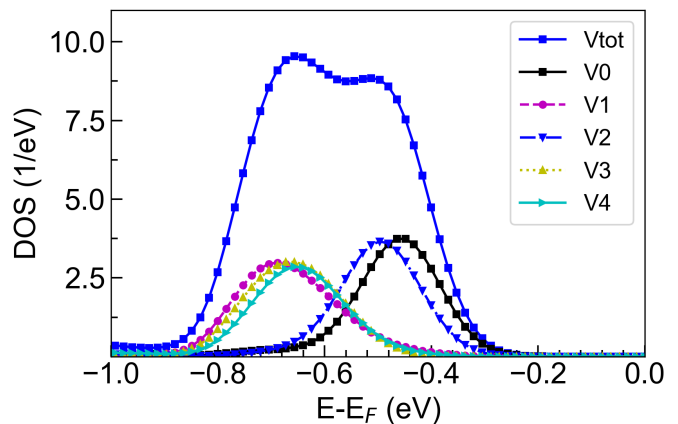


FIG. 6. Projection on V atoms of the occupied majority DOS near E_F for $n=5$.

out. These components sum up to produce about two-thirds of the total DOS, the rest coming from oxygen (see Figure 5). Quite analogous results are obtained for other concentrations and configurations.

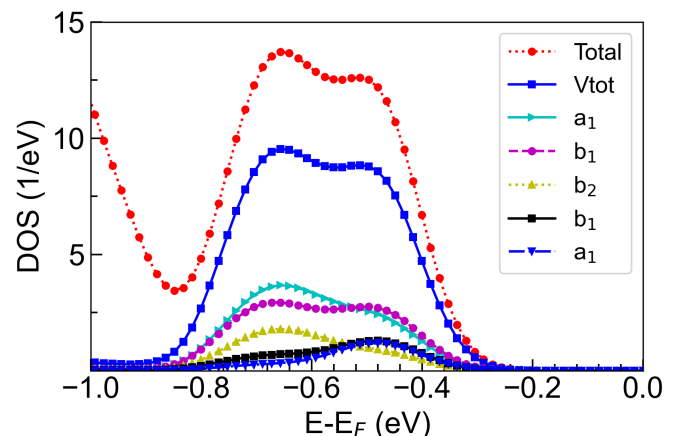


FIG. 7. Orbital-resolved V-projected DOS of the upper occupied states for $n=5$.

Figure 7 shows the orbital character of the occupied V-like gap states, again in the lowest-energy $n=5$ configuration. As mentioned, the V weight is almost totally d -like, and all the states resulting from the split d manifold are being admixed. At lower concentration the admixture is similar, though perhaps less marked.

Concerning optical response, dipole-allowed absorption in HfO_2 occurs in the UV between occupied O p and empty Hf d bands. As just shown, the states appearing in the HfO_2 gap upon V doping have V d character, which would imply dipole-forbidden transitions, hence no absorption. However, the $mm2$ point symmetry does not conserve parity, so that [22] certain transitions would be dipole-allowed depending on light polarization. The discussion of these effects [23] would be complicated by the fact that the reference axes vary locally from one V to the other in principle. Luckily, however, we need not go

into it, because symmetry is completely removed in our system due to disorder by random V substitution and attendant local distortions, so that no selection rules apply other than spin conservation.

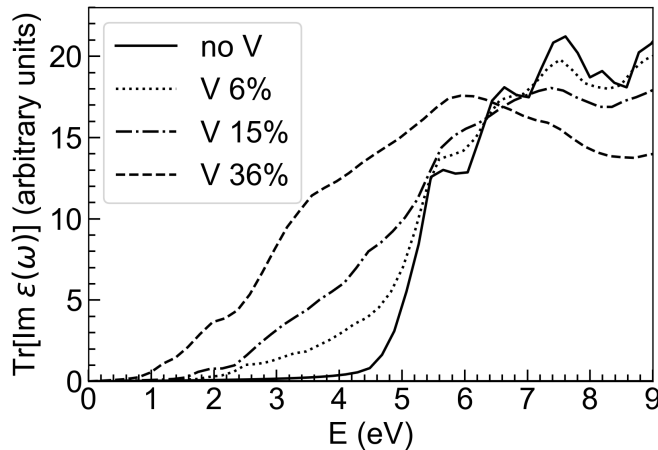


FIG. 8. Trace of the imaginary part of the dielectric function tensor at different V concentrations.

While a detailed treatment is outside our scope, we can get an idea of the absorption spectrum from Figure 8, which reports the trace (analogous to a Maxwell-Garnett average) of the imaginary dielectric-function tensor for $x=0, 6, 15, 36\%$. Clearly, the absorption onset of hafnia is at the DOS gap of about 4.9 eV as expected. The doped system shows absorption proportional to V concentration at lower energies: the onsets are at the DOS gaps of 1.9, 1.4, and 0.8 eV for $x=6, 15, 36\%$, and some higher absorptions (clearly visible at 6 %) appear near 2.5 and 3 eV as expected.

E. Connection to experiment

There are no experiments on $(\text{Hf},\text{V})\text{O}_2$, with the important exception of a very recent demonstration of a metal-ferroelectric-metal stack involving ferroelectric HfO_2 doped with V [4] (we became aware of that work while at an advanced drafting stage of this paper). Concentrations in the 3% to 11% range were investigated, all of them with analogous ferroelectric properties (all within our estimated stability range), the optimal performance being obtained [4] at 6% V and 900 K annealing. The temperature of 1000 K we used for weighting and entropic contributions is not far from those in [4]: the atomic-layer deposition growth is 515 K, and annealing was done between 700 and 1000 K. The immediate substrate layer for the $(\text{Hf},\text{V})\text{O}_2$ film is a TiN layer radiofrequency-sputtered on silica, presumably disordered. Our free-standing simulated cell may then be a not too inappropriate model for the hafnia overlayer.

The typical remnant polarization during testing was between 15 and 25 $\mu\text{C}/\text{cm}^2$, as was the saturation polarization. This is in quite decent agreement with the typi-

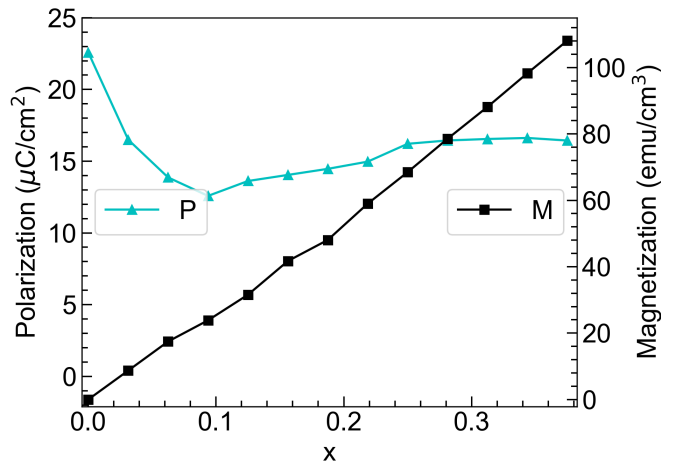


FIG. 9. P (left y axis) and total M (right y axis) in human units vs. concentration.

cal polarization predicted here, as can be seen in Figure 9, which reports polarization and magnetization in standard units. The magnetization vs x (also in Figure 9) is $M(x) \simeq 290 x \text{ emu}/\text{cm}^3$, so at the predicted stability limit of 16%, $M \simeq 46 \text{ emu}/\text{cm}^3$, and at the 6% V adopted in [4] M is a still respectable 17 emu/cm^3 .

This prediction applies to a state in which all V is acting as a 4+ ion. The XPS performed on samples at 6% and 11% V suggest that about two thirds (estimated from Fig.S1 of [4]) of the V atoms have 3+ valence, and one third have 4+. Valence 3+ corresponds to V_2O_3 local composition, and involves the formation of O vacancies in the HfO_2 matrix to maintain neutrality and insulating character. (This is indeed the only possible route in a dioxide when the substituting cation is purely 3+, as found long ago for Y-stabilized zirconia [24] and hafnia-alumina mixtures [25].) A description of the mixed valence system is outside our present scope, but our results prove that V can act as a 4+ ion and still produce an insulating and ferroelectric state in HfO_2 without compensating defect such as vacancies, which explains the otherwise puzzling one-third population of 4+ V ions.

Notably, the V 4+ ion is magnetic in the dioxide (whereas the 3+ is not, in the local sesquioxide stoichiometry facilitated by O vacancies). Based on our results, assuming the ratio of 3+ to 4+ V is indeed 2:1 as inferred from XPS, the samples of Ref.[4] with 3% to 11% V should already exhibit a magnetization of 3 to 11 emu/cm^3 . Further, an increase of the oxygen partial pressure (O-rich conditions) during growth will decrease the concentration of O vacancies, hence increase the fraction of magnetic 4+ V ions and hence the magnetization, potentially up to saturation at its full value (although some oxygen deficiency seems to be required to stabilize the hafnia polar phase). Of course, V acting as 4+ has a formation energy independent of O chemical potential, as in Eq.1. It barely needs specifying that no action is, or needs to be, taken to enforce a specific charge state of the V ion,

which adapts automatically to the chemical environment.

F. Structure

The large number of configurations makes an analysis of possible structural patterns quite difficult. We elect to inspect some of the low-energy structures for a few concentrations. The result is hard to convey visually, but analyzing the cells in 3D it is quite evident that V has a tendency, as concentration increases, to order first in rows (a trend noted earlier in [26]), then in multiple rows leading to incomplete or almost complete planes, then to multiple incomplete and "decorated" planes, which tend to stack along the \mathbf{b} and (to a lesser extent) the \mathbf{a} crystal axes. We attempt a summary in Figures 10 and 11, showing $2 \times 2 \times 2$ replicas of the simulation cell from a point of view in the first Cartesian octant near the xy plane. The vertical axis is the y direction. Only V-centered polyhedra are shown.

Figure 10 displays the lowest energy structures for $n=2, 3, 9$ and 11 . Clearly the structures mutate from rows ($n=2$) to intersecting rows forming largely incomplete planes ($n=3$), towards incomplete, decorated planes ($n=9$) to practically complete planes with decorations above and below ($n=11$, as well as $n=12$ in Figure 11). For the latter two, for example, there are 7 V in one plane with 8 cation sites per cell, which is a rather good guess at a "layered segregated" structure considering the totally random process leading to it and the fact that our

random-sample size is ~ 100 out of a binomial configurational spaces of size ranging from many thousands to several hundred millions for our concentrations.

Finally, in Figure 11 we compare the highest-energy structures with the lowest-energy ones in the cases $n=5$ and $n=12$. The differences again are that V clustering is less compact in the high-energy cases, while almost complete planes tend to emerge in the low-energy one.

IV. SUMMARY AND ACKNOWLEDGMENTS

Based on extensive ab initio calculations we have shown that ferroelectric HfO_2 mixed with vanadium up to 30% conserves a major fraction ($\sim 70\%$) of its polarization while acquiring a respectable ferromagnetic magnetization proportionally to V content (~ 2.9 emu/cm³ per V %). The mixing free energy indicates phase stability against the binary compounds (in the respective structures) up to around 16% V. Good agreement is found with a very recent experiment. $(\text{Hf,V})\text{O}_2$ then emerges as a robust ferromagnetic multiferroic with substantial magnetization and polarization, and thus promising for applications. The data supporting the findings above are openly available [27].

We thank Andrea Urru, Niccolò Martinolli, and Alessio Filippetti for a critical reading, and CINECA Bologna for the ISCRA Supercomputing Grant MAFNIA2 on EuroHPC Leonardo. VF thanks Università di Cagliari for a sabbatical leave and TU Dresden for a Senior DRESDEN Fellowship. VF and PA dedicate this paper to the memory of dr. Silvia Piacentini.

-
- [1] F. R. Theobald, R. Cabala, and J. Bernard, *Essai sur la structure de VO_2* , J. Sol. St. Chem. **17**, 431 (1976); As. Kumar, Ak. Kumar, A. Kandasami, and V. R. Singh, *A Comprehensive Review on Synthesis, Phase Transition, and Applications of VO_2* , J. Supercond. Novel Magn. **37**, 475 (2024); Materials Project, material mp-541404 at <https://tinyurl.com/4munzjrc>.
- [2] V. Eyert, *VO_2 : A Novel View from Band Theory*, Phys. Rev. Lett. **107**, 016401 (2011).
- [3] B. Noheda and J. Iñiguez, *A key piece of the ferroelectric hafnia puzzle*, Science **369**, 1300 (2020); Hyun-Jae Lee *et al.*, *Scale-free ferroelectricity induced by flat phonon bands in HfO_2* , Science **369**, 1343 (2020); I. Fina and F. Sanchez, *Epitaxial Ferroelectric HfO_2 Films: Growth, Properties, and Devices*, ACS Appl. Electron. Mater. **3**, 1530 (2021); S. Zhou, J. Zhang, and A. M. Rappe, *Strain-induced antipolar phase in hafnia stabilizes robust thin-film ferroelectricity*, Sci. Adv. **8**, eadd5953 (2022); S. Fan *et al.*, *Vibrational fingerprints of ferroelectric HfO_2* , npj Quantum Materials **7**, 32 (2022). A. Raeliarijaona and R. E. Cohen, *Hafnia HfO_2 is a proper ferroelectric*; Phys. Rev. B **108** 094109 (2023); B. Noheda, P. Nukala, and M. Acuaula, *Lessons from hafnium dioxide-based ferroelectrics*, Nature Materials **22**, 562 (2023); K. P. Kelley *et al.*, *Ferroelectricity in hafnia controlled via surface electrochemical state*, Nature Materials **22**, 1144 (2023); H. Alex Hsain *et al.*, *Wake-up free ferroelectric hafnia-zirconia capacitors fabricated via vacuum-maintaining atomic layer deposition*, J. Appl. Phys. **133**, 225304 (2023); M. Halter *et al.*, *A multi-timescale synaptic weight based on ferroelectric hafnium zirconium oxide*, Commun. Materials **4**, 14 (2023). S. Fan *et al.*, *Vibrational fingerprints of ferroelectric HfO_2* , npj Quantum Materials **7**, 32 (2022).
- [4] E. Ansari, N. Martinolli, E. Hartmann, A. Varini, I. Stolichnov, and A. M. Ionescu, *Vanadium-doped hafnium oxide: a high-endurance ferroelectric thin film with demonstrated negative capacitance*, Nano Lett. **25**, 2702 (2025).
- [5] G. Kresse and J. Furthmüller, *Efficient iterative schemes for ab initio total-energy calculations using a plane-wave basis set*, Phys. Rev. B **54**, 11169 (1996).
- [6] P. E. Blöchl, *Projector augmented-wave method*, Phys. Rev. B **50**, 17953 (1994); G. Kresse and D. Joubert, *From ultrasoft pseudopotentials to the projector augmented-wave method*, Phys. Rev. B **59**, 1758 (1999).
- [7] R. D. King-Smith and D. Vanderbilt, *Theory of polarization of crystalline solids*, Phys. Rev. B **47**, 1651

- (1993); R. Resta, *Macroscopic polarization in crystalline dielectrics: the geometric phase approach*, Rev. Mod. Phys. **66**, 899 (1994); R. Resta and D. Vanderbilt, *Theory of Polarization: A Modern Approach*, in *Physics of Ferroelectrics: A Modern Perspective*, K. Rabe, C. H. Ahn, J.-M. Triscone eds., Topics Appl. Physics **105**, 31 (2007).
- [8] J. P. Perdew, K. Burke, and M. Ernzerhof, *Generalized Gradient Approximation Made Simple*, Phys. Rev. Lett. **77**, 3865 (1996).
- [9] S. L. Dudarev, G. A. Botton, S. Y. Savrasov, C. J. Humphreys, and A. P. Sutton, *Electron-energy-loss spectra and the structural stability of nickel oxide: An LSDA+U study*, Phys. Rev. B **57**, 1505 (1998).
- [10] J. Heyd, G. E. Scuseria, and M. Ernzerhof, *Hybrid functionals based on a screened Coulomb potential*, J. Chem. Phys. **118**, 8207 (2003).
- [11] Muratahan Aykol and C. Wolverton, *Local environment dependent GGA+U method for accurate thermochemistry of transition metal compounds*, Phys. Rev. B **90**, 115105 (2014); A. Jain, G. Hautier, S. P. Ong, C. Moore, C. Fischer, K. A. Persson, and G. Ceder, *Formation enthalpies by mixing GGA and GGA+U calculations*, Phys. Rev. B **84**, 045115 (2011); see also the Materials Project docs at <https://tinyurl.com/bdxz6ech>.
- [12] G. Scarel, C. Wiemer, S. Ferrari, G. Tallarida, and M. Fanciulli, *Effects of growth temperature on the properties of HfO₂ films grown by atomic layer deposition*, Proc. Estonian Acad. Sci. Phys. Math. **3**, 308 (2003); C. V. Raman, K. Kamala Bharathi, A. Garcia, and A. L. Campbell, *Growth Behavior, Lattice Expansion, Strain, and Surface Morphology of Nanocrystalline, Monoclinic HfO₂ Thin Films*, J. Phys. Chem. C **116**, 9955 (2012); T. Gougousi, *Low-Temperature Dopant-Assisted Crystallization of HfO₂ Thin Films* Crystal Growth & Design **21**, 6411 (2021); S. Yang, D. Lehninger, A. Sünbül, F. Schöne, A. Reck, K. Seidel, G. Gerlach, and M. Lederer, *Crystalline phase control of ferroelectric HfO₂ thin film via heterogeneous co-doping*, Appl. Phys. Lett. **125**, 132903 (2024); M. Beedel, M. A. Rahman, H. Farkhondeh, J. P. Thomas, L. Zhang, N. F. Heinig, and K. T. Leung, *Single-crystalline HfO₂ nanostructures with novel ferromagnetic properties*, Materials Today Nano **28**, 100510 (2024).
- [13] See e.g. Fig.1 in Y. Liang, P. Qin, Z. Liang, X. Yuan, and Y. Zhang, *Identification of a monoclinic metallic state in VO₂ from a modified first-principles approach*, Mod. Phys. Lett. B **33**, 1950148 (2019).
- [14] A. Jain, S. P. Ong, G. Hautier, W. Chen, W. D. Richards, S. Dacek, S. Cholia, D. Gunter, D. Skinner, G. Ceder, and K. A. Persson, *The Materials Project: A materials genome approach to accelerating materials innovation*, APL Mater. **1**, 011002 (2013).
- [15] H. Aramberri and J. Iñiguez, *Theoretical approach to ferroelectricity in hafnia and related materials*, Commun. Mater. **4**, 95 (2023).
- [16] C.H.P. Lupis, *Chemical Thermodynamics of Materials* (Prentice Hall, 1993); <https://tinyurl.com/2x6adz4>.
- [17] M. B. Maccioni and V. Fiorentini, *Phase diagram and polarization of stable phases of (Ga_{1-x}In_x)₂O₃*, Appl. Phys. Expr. **9**, 041102 (2016); M. B. Maccioni, F. Ricci and V. Fiorentini, *Properties of (Ga_{1-x}In_x)₂O₃ over the whole x range*, J. Phys.: Condens. Matter **28**, 224001 (2016).
- [18] For $x>0$, a function x^a with $0<a<1$ is upward convex and monotonically increasing, whereas if $1<a$ it is downward convex.
- [19] F. Ricci and V. Fiorentini, *Multiferroicity in V-doped PbTiO₃*, J. Phys.: Conf. Series **470**, 012013 (2013).
- [20] C. Bhandari and W. R. L. Lambrecht, *Phonons and related spectra in bulk and monolayer V₂O₅*, Phys. Rev. B **89**, 045109 (2014).
- [21] A. Filippetti and V. Fiorentini, *A practical first-principles band-theory approach to the study of correlated materials*, Eur. Phys. J. B **71**, 139 (2009); A. Filippetti, C. D. Pemmaraju, S. Sanvito, P. Delugas, D. Puggioni, and V. Fiorentini, *Variational pseudo-self-interaction-corrected density-functional approach to the ab-initio description of correlated solids and molecules*, Phys. Rev. B **84**, 195127 (2011).
- [22] M. S. Dresselhaus, G. Dresselhaus, and A. Jorio, *Group Theory: Application to the Physics of Condensed Matter* (Springer, New York-Berlin 2008).
- [23] The transitions $a_1 \rightarrow b_1$, $a_1 \rightarrow b_2$, and $a_1 \rightarrow a_1$ are allowed for polarization along the local octahedron axes $\hat{x}=\mathbf{o}_1$, $\hat{y}=\mathbf{o}_2$, and $\hat{z}=\mathbf{o}_3$ respectively. For octahedra all oriented equally, since the highest occupied state is expected to be a_1 and the empty ones to be b_1 , b_2 and a_1 (from the e_g manifold), dipole absorption for \mathbf{o}_1 -polarized and \mathbf{o}_2 -polarized light is expected starting at around 1 eV, depending on V concentration, while absorption of \mathbf{o}_3 -polarized light should show up at higher (around 3 eV) energies corresponding to a transition from a_1 to the formerly- e_g state a_1 .
- [24] A. Eichler, *Tetragonal Y-doped zirconia: Structure and ion conductivity*, Phys. Rev. B **64**, 174103 (2001).
- [25] M. Alessandri, R. Piagge, S. Alberici, E. Bellandi, M. Canniatti, G. Ghidini, A. Modelli, G. Pavia, E. Ravizza, A. Sebastiani, C. Wiemer, S. Spiga, M. Fanciulli, E. Cadelano, G. M. Lopez, and V. Fiorentini, *High-k materials in FLASH memories*, in *Physics and Technology of High-k Gate Dielectric III*, ECS Trans. **1**, 91 (Electrochemical Society, 2006).
- [26] M. Scarozza, A. Filippetti, and V. Fiorentini, *Ferromagnetism and orbital order in a topological ferroelectric*, Phys. Rev. Lett. **109**, 217202 (2012); *Multiferroicity in vanadium-doped La₂Ti₂O₇: insights from first principles*, Eur. Phys. J. B **86**, 128 (2013).
- [27] A zipped tar file ($\simeq 500$ Mb in total) with final cell and positions, energy, polarization, magnetization, DOS of all studied (Hf,V)O₂ configurations for $n=1$ to 12 is at <https://tinyurl.com/bdhw967>. A README and the main postprocessing Python scripts are included. The computational details in the paper and the cell/positions files are sufficient to reproduce the calculations with VASP. The other data (extracted from the full output) and the scripts can be used to reproduce the Figures. The full output is over 300 Gb and can be made available on request. A further 800 Gb (wavefunctions, charge) was deleted, but can be regenerated. PAW potential datasets cannot be made available because they are licensed by VASP and are not public.

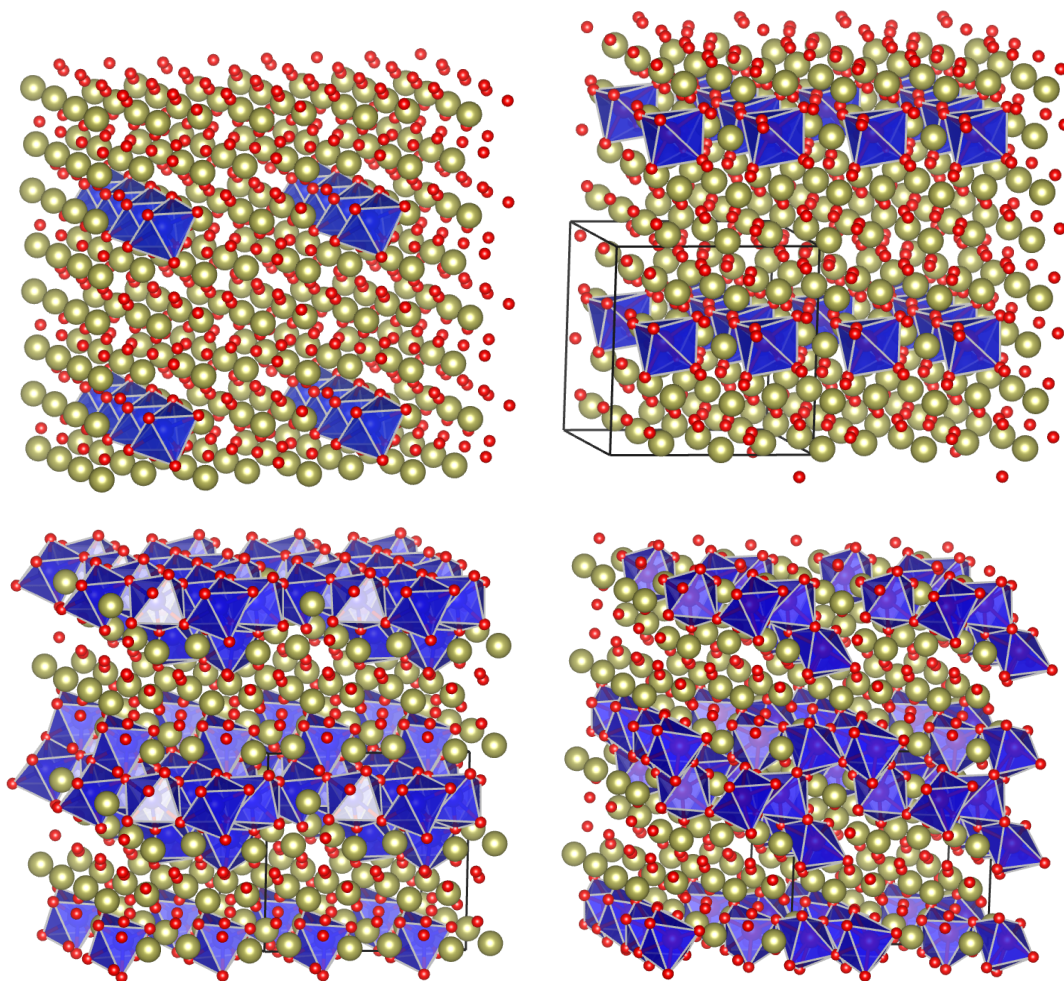


FIG. 10. Minimum-energy structures for $n=2, 3, 9, 11$ (clockwise from top left), viewed from a direction in the first octant. The vertical direction is y .

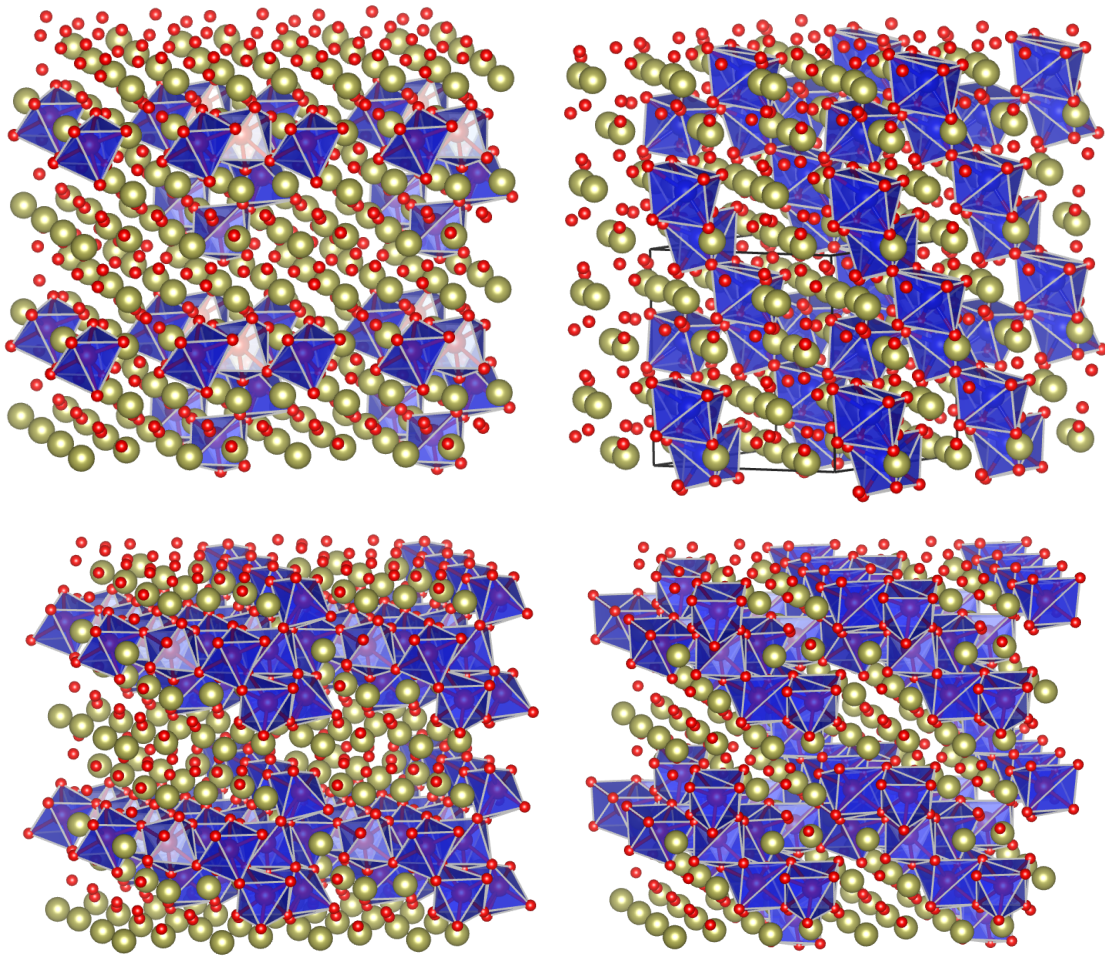


FIG. 11. Minimum-energy (left) vs maximum-energy (right) structures for $n=5$ (top) and $n=12$ (bottom). Same view as the previous Figure. The vertical direction is y .